

# CANLab2025: A multiscale probabilistic meta-atlas of the healthy human brain

**Bogdan Petre (bogdan.petre@dartmouth.edu)**

Department of Psychological and Brain Sciences, Dartmouth College  
3 Maynard Street, Hanover, NH 03755 USA

**Martin A Lindquist (mlindqui@jhsph.edu)**

Department of Biostatistics, Johns Hopkins University  
615 N Wolfe Street, Baltimore, MD 21205 USA

**Tor D Wager (tor.d.wager@dartmouth.edu)**

Department of Psychological and Brain Sciences, Dartmouth College  
3 Maynard Street, Hanover, NH 03755 USA

## Abstract

[Say something about the total number of regions, number of constituent atlases, and formats/templates in which CANLab2025 is available. Consider renaming the atlas to recognize the community more. Maybe HBA2025 (human brain atlas 2025), or, taking a cue from MNI, DHBA2025 (Dartmouth Human Brain Atlas 2025). The latter might require reaching out to more people in the Dept for feedback though...]

**Keywords:**

## TODO

Add grayordinate surface/volume overlap illustration for hippocampus/amygdala and caudate/putamen  
complete missing structural descriptions in methods  
Evaluate registration fusion in spacetime, bmrk5 and pain-gen task contrast specificity (results: cortex section)  
Find reference for cifti structural labels being T1 contrast based (results: basal ganglia section)  
Do spatial comparisons of brainstem atlases, and PET based validations (results: brainstem section).  
Create README in CANLab2024/2025 directories

## Introduction

Human neuroscience needs a reference ontology of brain structures when designing or reporting experiments, describing clinical pathology or measuring signals of interest in a consistent way across people. This need has traditionally been met by printed stereotactic references atlases combined with classic histological labeling schemes, e.g. of Brodmann or Von Economo (Mai, Paxinos, & Voss, 2008; Talairach & Tournoux, 1988), and is now served by digitized brain atlases with improved precision and detail. A large number of competing labeling schemes are available and widely distributed, often alongside popular neuroimaging software which contributes to their adoption. Examples include the gyral/sulcal cortical surface atlases and subcortical volumetric atlases packaged with FreeSurfer (Fischl et al., 2002; Klein & Tourville, 2012; Desikan et al., 2006; Destrieux et al., 2010), Brodmann like histological maps (Amunts et al., 2020) or the Harvard-Oxford cortical and subcortical atlases packaged with

FMRIB's FSL. Different atlases are defined according to different criteria including anatomical folding patterns (Klein & Tourville, 2012; Desikan et al., 2006; Destrieux et al., 2010), white matter tractography (Cartmell et al., 2019), histology and immunohistochemistry (Edlow et al., 2012, 2023; Amunts et al., 2005, 2020; Iglesias et al., 2018), functional topographies (Glasser et al., 2016) and network based metrics (Shen et al., 2013), providing users with a large selection of flexible parcellations suitable for a variety of uses.

The proliferation of atlases has yet to be reconsolidated into a standard general purpose anatomical ontology. This is in part a technical problem. The most accessible atlases (FSL's and Freesurfer's) are relatively coarse and fail to take advantage of the latest developments in human brain mapping. Additionally, most atlases lack full brain coverage. In most cases the most detailed atlases for any gross brain structure (e.g. cortex, brainstem, etc.) are more detailed than competing full brain atlases, but show varying degrees of overlap and are registered to distinct reference spaces, which makes them difficult to combine in practice for both comprehensive and detailed characterization of brain function. Some also face licensing restrictions on usage or distribution which impedes incorporation into comprehensive atlases. This encourages investigators to use vague or incommensurate labeling schemes, and impedes cumulative scientific discoveries.

We propose a comprehensive brain atlas should meet several criteria. (1) Be granular and detailed to allow for the most precise description of locations in the brain. (2) Provide full brain coverage from the medulla to the cortex. (3) Be compatible with popular but differing reference spaces for flexible use across software environments, analysis pipelines and imaging modalities. (4) Provide probabilistic labels that convey boundary ambiguities and facilitate modifications like principled regional erosion, substitutions, and Bayesian segmentations. (5) Be openly licensed for broad and unrestricted use. (6) Be suitable for both ontological attribution and region of interest selection for robust signal extraction. (7) Be packaged in file formats that abide by the NIFTI, GIFTI and CIFTI neuroimaging data standards.

Here we address a number of technical and legal obstacles to present a combined meta-atlas that offers a comprehen-

sive reference suitable for general use. Our atlas incorporates many atlases already widely embraced by the neuroimaging community, as well as the most modern atlases available for each brain structure we evaluate. It combines noninvasive structural, functional, tractography and invasive histological data to delineate 358 unique cortical (Human Connectome Project Multimodal Parcellation, HCP-MMP, 1.0) and 160 subcortical structures. We believe that proposals of comprehensive atlases of this kind can move us closer to a standardized ontology of the human brain that meets the demands of modern brain mapping. We call ours the CANLab2025 atlas.

Our atlas balances across our idealized goals in a parsimonious way by using a suite of interchangeable variants. openCANLab2025 forms the basis of these variants and includes only openly licensed atlases. It is directly available from our github repository. CANLab2025 augments openCANLab2025 with additional brainstem areas that are subject to distribution restrictions, but are more granular than any other digitized brain segmentation. This atlas is available in the form of matlab code that automatically assembles CANLab2025 by combining openCANLab2025 with online resources obtained from properly licensed sources. Additionally, atlas parcellations are available at multiple nested scales of granularity. We anticipate more granular atlases will be suitable for signal attribution and "reverse inference", i.e.  $P(\text{region} \mid \text{activation})$ , but we also curated less granular parcellations to provide more robust use in ROI based signal estimation, as tractography targets, and in forced-choice discrete parcellation schemes. Labels are available in register with volumetric MNI152NLin6Asym (RAS) and MNI152NLin2009cAsym (RAS and LPS oriented) templates and HCP 91k grayordinate space (which subsumes FreeSurfer's fsLR surfaces). Finally, we provide resampled atlases at both 1mm and 2mm spatial resolution which were specifically generated using techniques that minimize interpolation related smoothing ("partial volume effects") and maximize equivalence across sampling resolutions. Although our atlas only includes gray matter structures, future atlases might additionally label white matter tracts.

Several constituent atlases used in (open)CANLab2025 needed format conversions for inter-atlas compatibility. Consequently, we also provide novel surface to volume projections of the Glasser cortical atlas (Glasser et al., 2016), novel voxel space definitions of the Freesurfer/Iglesias thalamic (Iglesias et al., 2018) and hypothalamic (Billot et al., 2020) parcellations, and the first public copy of a probabilistic Tian subcortical segmentation (Tian, Margulies, Breakspear, & Zalesky, 2020). In the most complex instances reference data was needed to calibrate voxel probabilities. Multimodal data from 716 participants spanning 4 previously published studies was incorporated to achieve this. We included data from the human connectome project (HCP)(Essen et al., 2013) and three in house studies we refer to as spatial topology (SpaceTop) (?), ?, pain genetics (PainGen) (Botvinik-Nezer et al., 2023) and biomarkers 5 (BMRK5) (Losin et al., 2020). These same studies were additionally used to validate the obtained projections.

This document details the procedures used for atlas projections, combination and validation of (open)CANLab2025 and constituent atlases.

## Methods

14 previously published atlases were used in (open)CANLab2025. These are detailed in Table 1. Of these Glasser, Tian, Freesufer/Iglesias, Freesurfer/Billot and KragelPAG required modifications to their labels that go beyond the versions thus far publicly available. These are described in corresponding subsections below. All atlases required alignment to several reference templates. The same tools were used for alignment for each atlas, which are described in the Atlas Registration section. Further registration details are provided for each constituent atlas in atlas specific subsections.

### Atlas Registration

**Full brain MNI-to-MNI** [Determine if the full brain alignment is used at all]

Nonlinear volumetric registration transforms between template spaces were computed by direct template-to-template registration. Templates used were non-skull stripped MNI152NLin6Asym, MNI152NLin2009cAsym and Colin27 (Holmes et al., 1998). MNI152-to-MNI152 template alignment underperforms relative to subject-to-MNI152 alignment because templates are averages of individual brains, any misalignment contributes to reduced contrast, and image contrast determines the features available for alignment. Low contrast images (MNI-to-MNI) are subsequently harder to bring into alignment than higher contrast images (subject-to-MNI). In other words, templates are more blurry than subject specific images. However, the effect is largest in cortical areas where idiosyncratic folding patterns lead to a high degree of misalignment, but relatively low in subcortical regions where volumetric structures are generally better aligned across individuals, and we only used MNI-to-MNI alignment for subcortical structures.

Unweighted full brain alignments were estimated by running fmriprep v20.2.3 (LTS) anatomical workflows on 1mm MNI templates obtained from TemplateFlow (MNI152 templates) or directly from the Montreal Neurological Institute (Colin27). These templates are provided in RAS orientation but for compatibility with QSIprep DWI pipelines we also need an LPS oriented atlas. Therefore we additionally obtained a copy of MNI152NLin2009cAsym in LPS orientation directly from the QSIprep github repository ([https://github.com/PennLINC/qsiprep/blob/master/qsiprep/data/mni\\_1mm\\_t1w\\_lps.nii.gz](https://github.com/PennLINC/qsiprep/blob/master/qsiprep/data/mni_1mm_t1w_lps.nii.gz)) to use as an alignment reference image as well.

**Subcortical MNI-to-MNI** Alignment involves estimating a transformation that minimizes a misalignment cost function. Alignment weight masks provide a mechanism for improving alignment within a target area by only penalizing misalignments within masked regions while ignoring misalignments of

Table 1: CANLab2025 constituent atlases

Structure	Atlas	Segmentation Modality	Reference	open-CANLab2025	CANLab2025
Cortex	Glasser	T1, T2, BOLD (Rest) BOLD (Task)	(Glasser et al., 2016)	Included	Included
Thalamus	Freesurfer/Iglesias	Histology, T1, DWI (FA & DTI)	(Iglesias et al., 2018)	Included	Included
Caudate, Putamen	Tian	BOLD (Rest)	(Tian et al., 2020)	Included	Included
Accumbens	Cartmell	DWI (Tractography)	(Cartmell et al., 2019)	Included	Included
Hypothalamus	Freesurfer/Billot	Histology	(Billot et al., 2020)	Included	Included
Amygdala	CIT168 amygdala v1.0.3	T1, T2	(Tyszka & Pauli, 2016)	Included	Included
Hippocampus	Julich/Amunts	Histology	(Amunts et al., 2005) (Amunts et al., 2020)	Included	Included
Cerebellum	SUIT	T1	(Diedrichsen et al., 2009)	Included	Included
PAG	KragelPAG	T1	(Kragel et al., 2019)	Included	Included
Pallidum, Subthalamus, Ventral diencephalic nuclei, Habenula, Extended amygdala	CIT168 subcortex v1.1.0	T1, T2	(Pauli et al., 2018)	Included	Included
Dorsal Raphe, ACh nuclei, Cranial nuclei	Levinson-Bari Limbic Brainstem Atlas	T1, T2	(Levinson et al., 2023)	Included	Included (Dorsal Raphe & ACh Nuclei)
5-HT nuclei, Tectal nuclei, Reticular formations, Olivary nuclei, ACh nuclei, Pontine nuclei, Cranial nuclei	Bianciardi v0.9	T1, T2, DWI	(Bianciardi et al., 2015) (Bianciardi et al., 2016) (Bianciardi et al., 2018) (García-Gomar et al., 2019) (Singh et al., 2020)	-	Included
ACh nuclei, Parabrachial complex, Pontine nuclei, Rostral reticulum	Harvard Asending Arousal Network v2.0	Histology	(Edlow et al., 2012, 2023)	Included	-
Brainstem Filler	Shen268	BOLD (Rest)	(Shen et al., 2013)	Included	Included

regions outside the mask. Weighted subcortical alignments were estimated using a multimodal alignment (T1 and T2) pro-

cедure similar to the one used by fmriprep, only with the CIFTI subcortical mask used as an alignment mask. antsRegistration

tion was used for registration with the following configuration. Note the use of the cifti\\_mask.nii.gz file. That is the subcortical mask.

```
$FIMG = <target T1 template>
$MIMG = <source T1 template>
$FIMG.T2 = <target T2 template>
$MIMG.T2 = <source T2 template>
antsRegistration -o [$outfile ,1,1]
--dimensionality 3
--transform Rigid[0.05]
--metric
    Mattes[$FIMG,$MIMG,1,32,Regular,0.25]
--convergence
    [1000x500x250x100,0.00000001,10]
--shrink-factors 8x4x2x1
--smoothing-sigmas 4x2x1x0vox
--use-histogram-matching 1
--masks [cifti_mask.nii.gz,NULL]
--transform Affine[0.1]
--metric
    Mattes[$FIMG,$MIMG,1,32,Regular,0.25]
--convergence
    [1000x500x250x100,1e-8,10]
--shrink-factors 8x4x2x1
--smoothing-sigmas 4x2x1x0vox
--use-histogram-matching 1
--masks [cifti_mask.nii.gz,NULL]
--transform SyN[0.1,3,0]
--metric
    CC[$FIMG,$MIMG,0.5,4,None,1]
--metric
    CC[$FIMG_T2,$MIMG_T2,0.5,4,None,1]
--convergence [50x10x0,1e-9,15]
--shrink-factors 4x2x1
--smoothing-sigmas 2x1x0vox
--use-histogram-matching 1
--masks [cifti_mask.nii.gz,NULL]
--winsorize-image-intensities
    [0.025,0.975]
```

**Surface to volume fsLR-to-MNI projection** We use registration fusion (Wu et al., 2018) to transform data between volumetric and surface spaces. Registration fusion uses subject specific surface to volume transformations to produce subject specific projections from surface templates to volumetric templates. Due to differences in cortical folding patterns across individuals, and variability in how the cortical sheet is embedded in 3d volumetric space, each surface parcel maps to slightly different locations in each participant's MNI152-registered brain volume. We computed surface to volume projections for 241 PainGen participants, 87 BMRK5 participants and 112 SpaceTop participants by running anatomical workflows in fmriprep 20.2.3 (LTS) with surface reconstruction enabled using both MNI152NLin2009cAsym and MNI152NLin6Asym as target volumetric templates. This produced native space to

fsaverage surface projections and native space to MNI152-template projections which we can enchain to transform deterministic surface parcels into subject specific volumetric parcel labels. Probabilities were assigned to each parcel label at each voxel coordinate based on the frequency with which that label was assigned to that voxel in each study. We then averaged probabilities across studies so that our labels would be more robust to variation across acquisition sequences, geographic locations and sample demographics. Our cortical parcel probabilities thus reflect the idiosyncrasies in cortical folding, while our surface parcellation is deterministic.

## Volumetric segmentations

**Thalamus** Thalamic probabilistic labels are not directly derived from the original parcellation (Iglesias et al., 2018) that is used internally by Freesurfer. Those probabilistic labels aren't readily available. They're stored in an esoteric format internally by Freesurfer. Instead, we fit the Freesurfer segmentation to new participants and incorporate the obtained labels into CANLab2025.

Freesurfer's Thalamic segmentation was run on T1 and DWI data from 278 unrelated HCP participants, 76 spacetop participants (all spacetop participants are unrelated) and 264 unrelated paingen participants. These samples were chosen because they had both DWI and T1 data available, both of which are needed to apply the most advanced and reliable versions of the Freesurfer segmentation algorithm. An additional subset of 138 unrelated HCP participants also had T1 and DWI available, but were omitted so that they could be used as an unseen validation sample in a separate study with which some of the authors are concurrently involved. The selection of subjects for this validation sample was made randomly. Our one remaining study, BMRK5, had only T1 data and was not segmented.

Both T1 and DWI data are needed for segmentation, but due to the different transformation formats, image orientations and data modalities we combined workflows from multiple pipelines to preprocess our data for segmentation.

SpaceTop and PainGen DWI data was preprocessed in parallel using both QSIprep (v0.16.1) and fMRIprep (v20.2.3). Fractional anisotropy (FA) was estimated using fsl 6.0.4's dtifit and QSIprep outputs. QSIprep transforms data to a consistent native space using rigid body alignments to the AC-PC axes and conversion to LPS+ orientation. FA data was transformed from this QSIprep "native space" to the original T1w image space for consistency with fMRIprep T1 outputs (SpaceTop and PainGen). This transformation was estimated based on T1w outputs of QSIprep and fMRIprep using antsRegistration with the following configuration,

```
FIMG = <fmriprep_T1w>
MING = <qsiprep_T1w>
antsRegistration
--dimensionality 3
--transform Rigid[0.2]
--metric
```

```

    Mattes[$FIMG,$MING,1,32,Random,0.25]
--convergence
[10000x1000x10000x10000,1e-06,10]
--smoothing-sigmas
7.0x3.0x1.0x0.vox
--shrink-factors 8x4x2x1
--use-histogram-matching 1
--winsorize-image-intensities
[0.025,0.975]

```

Transformations were applied to scalar valued data using antsTransform. Transformations were converted from ANTs to FSL format using ITK-SNAP's Convert3D Medical Image Processing Tool (v1.1.0) and applied to vector valued data using FSL's vecreg tool. Data was upsampled using b-spline interpolation in both cases.

For HCP the minimally preprocessed data was used. This data has been brain extracted, distortion corrected, cropped and rigid body transformed to align acpc axes (Glasser et al., 2013). Additionally, transformations from this space to MNI152NLin6Asym are precomputed by HCP. QSIPrep (v0.16.1) was additionally run on the unaligned data to obtain transformations to MNI152NLin2009cAsym space. Transformations from HCP ACPC space to QSIPrep native space were computed using the same antsRegistration options listed above for transformations between QSIPrep to fMRIPrep spaces, only with the HCP T1w acpc\_dc image used as the moving image (\$MING) and the QSIPrep T1w image used as the fixed image (\$FIMG). Data was transformed into MNI152NLin2009cAsym space by enchaining this transformation with the QSIPrep T1w-to-MNI152NLin2009cAsym transformation. In principle we could have taken a more direct approach and simply computed the HCP ACPC to MNI152NLin2009cAsym transformation directly, but nonlinear transformations of this variety are complex to configure and it seemed safest to reuse established approaches like QSIPrep's dtifit was run in the HCP ACPC space.

Segmentations were performed using Freesurfer 7.4.1's mri\_segment\_thalamic\_nuclei\_dt1\_cnn with the v1.1 model patch (H. F. Tregidgo et al., 2023; H. F. J. Tregidgo et al., 2023). Segmentation was performed in HCP acpc\_dc space or FMRIPrep's native space (SpaceTop and PainGen). Spatial transformations to MNI152NLin6Asym and MNI152NLin2009cAsym templates were applied to obtained labels using NearestNeighbor interpolation. Label incidence across participants was used to derive study specific label probabilities, which were then averaged to obtain probabilistic maps in MNI152NLin6Asym and MNI152NLin2009cAsym spaces. These differ from direct transformations of probabilistic labels between MNI templates because probability distributions differ as a function of alignment consistency, and alignment consistency is greater for the newer MNI152NLin2009cAsym template than the older and lower contrast MNI152NLin6Asym template. This difference should reflect variability in subnuclear locations in samples registered to either template.

## Atlas Components

**Cortex (Glasser)** Cortical parcels are all obtained from (Glasser et al., 2016), a deterministic parcellation of the cortical surface based on T1/T2 contrast ratio (a proxy for myelin), cortical folding, resting state networks and task evoked responses across seven tasks (working memory, motor, emotional faces, theory of mind, relational, gambling, language). These features are available at the subject level and Glasser et al. developed feature based classifiers for individualized parcellations, but to our knowledge these classifiers and individualized parcellations have never been released. They additionally produced volumetric projections of these parcels (Coalsen et al., 2018), but this has also never been released to the public. Instead, we adopt their deterministic surface parcellation and produced our own volumetric projections using registration fusion (Wu et al., 2018).

Surface to volume projection revealed the hippocampus parcel (Ctx.H in the original labeling scheme) overlapped with volumetric grayordinate coordinates. In other words, the hippocampus has redundant representations in HCP 91k grayordinate space as both surface vertices and volumetric voxels (Figure ??). To reconcile this disparity we deleted the hippocampal surface parcel from the Glasser parcellation, and retained only the remaining 358 bilateral regions. The complete hippocampal parcellation, including segmented hippocampal subfields, was left for other atlases to define (below). For select participants the ?entorhinal? cortex may also overlap with volumetric grayordinates, but we found this overlap was limited and only occurred in a minority of participants, so we did not modify the entorhinal parcels.

The Glasser parcellation lent itself naturally to two levels of granularity. (Glasser et al., 2016) group their parcels both by their choice of color scheme (reproduced in Figure 1) and in their supplemental methods into 23 discrete categories of contiguous regions, which we adopted as our coarsest parcellation (level 3 and level 4). We drew no distinctions between the finest two levels of granularity (levels 1 and 2), which simply reproduce the Glasser parcellation.

**Caudate/Putamen (Tian)** [discuss erosion of the most lateral parts of the Putamen]

**Pallidum (CIT168 subcortical)** The CANLab2025 pallidum is derived from the CIT subcortical atlas and includes internal, extrenal and ventral segments. The ventral pallidum is quite small (<10 voxels at 2mm resolution), so at granularity level 2 it was combined with the external segment. This choice was made based on histological markers (enkephalin and dynorphin like immunoreactivity) and cytoarchitectural features (woolly fibers) that are shared by ventral pallidum with the external but not internal primate pallidal segments (S. Haber & Watson, 1985; Reiner et al., 1999). This assignment may be a bit misleading though. Functionally, internal and external segments of the dorsal globus pallidus correspond to direct and indirect pathways of cortico-basal ganglia-thalamocortical

circuits, but in the ventral pallidum no such neat distinction is available and different subpopulations of neurons project to both the ventral tegmentum (indirect) and the mediodorsal nucleus of the thalamus (direct) (Leung & Balleine, 2015). We simply pick the best of two lousy choices.

**Accumbens (Cartmell)** The accumbens is subdivided into core and shell regions based on a diffusion tractography segmentation in 245 unrelated HCP participants, validated using MRI based functional and microstructural measures, post-mortem immunohistochemistry, cross species comparisons, and differential affective responses to deep brain stimulation in human patients (Cartmell et al., 2019). The right accumbens core in this parcellation contained two spatially disconnected set of voxels, one large ( $624\text{mm}^3$ ) and one small ( $24\text{mm}^3$ ). The latter was reassigned to right shell. Additionally, voxels intersecting with the bed nucleus of the stria terminalis and subtenuicular extended amygdala (BST\_SLEA) of CTI168 (Pauli et al., 2018) were assigned to the latter. Finally, any remaining voxels of the CIFTI "accumbens" structure were assigned by nearest neighbor dilation of shell, core and BST\_SLEA.

**Amygdala (CIT168 amygdala)** [intercalated nuclei are only available in the fine 1mm atlas]

**Hippocampus (Julich/Amunts)** [Our labeling scheme defines "hippocampal formation" as CA1-3, DG and subiculum, but not entorhinal cortex, and our generic "hippocampus" label includes the DG in addition to CA1-3, even though only CA1-3 are considered 'hippocampus proper'. These labels were driven by practical considerations, not physiological ones.]

**Thalamus (Iglesias2018)** [Nucleus reunies, one of the interlaminar nuclei, is only available in the 1mm fine parcellation. Habenula is nested within the coarser thalamic parcellations, but we discuss it with the subcortical nuclei since we obtain it from CIT168 subcortical.]

**Hypothalamus (Billot2020)** asdf

**Cerebellum (SUIT)** Cerebellar parcels were defined by lobular and vermal segmentation based on T1 contrast (Diedrichsen et al., 2009). The resultant parcels were relatively large to begin with, and we did not further downsample them at level 2 of granularity, but grouped them at level 3 into four larger parcels by combining three ventral parcels (lobules I, IV, V and VI), 3 caudal parcels (crus I and II, and lobule VIIb) and 3 dorsal parcels (lobules IX, X VIIIa and VIIb) and all vermal parcels. This lobular division was chosen to correspond to previously reported topographic differences

in cortico-cerebellar functional networks, since crus I, II and lobule VIIb shows greater default mode network connectivity while surrounding areas show greater salience, sensorimotor and visual network connectivity (Xue et al., 2021). Level four subdivides the cerebellum into lateralized cortical parcels and a vermal parcel.

The source parcellation (Diedrichsen et al., 2009) also includes deep cerebellar nuclei. These were not included here because they are not represented in HCP 91k grayordinate space and would have introduced a significant discrepancy across formats of (open)CANLab2025.

**PAG (KragelPAG)** The periaqueductal gray matter (PAG) was defined literally by using T1 contrast to segment the cerebral aqueduct and assign any voxel within 2mm to the PAG. Subcolumns were identified based on spatial location along the PAG's angular axis, and segmentations were validated based on noninvasive but fine scale (1.1mm isotropic, 7T, blood oxygen level dependent) functional measures (Kragel et al., 2019). Label probability values were assigned based on unpublished subject level segmentations (N=19) obtained from the authors of (Kragel et al., 2019). These did not distinguish subcolumns, so intercolumnar boundaries are deterministic, while PAG-nonPAG boundaries are probabilistic. These segmentations were originally aligned to the MNI152NLin6Asym template, and transformed to MNI152NLin2009cAsym using a subcortically weighted alignments. [Note that the PAG incorporates Cuneiform nucleus from Bianciardi in CANLab2025, but not openCANLab2025]

**Subcortical nuclei (CIT168 subcortical)** [The habenula was reassigned to the medial pulvinar at levels 2-4 of granularity]

**Brainstem Nuclei (Bianciardi v0.9)** [Note that Cuneiform nucleus is merged with PAG at level 2 and higher. Alternative nearby nuclei are the superior and inferior colliculi, but PAG seems more functionally similar given their shared involvement in pain. The superior olfactory complex and the inferior olfactory nucleus are also merged at level 2. These are functional distinct regions but are in close proximity and difficult to distinguish at 2mm isotropic resolutions.]

**Brainstem Nuclei (Levinson-Bari)** asdf

**Brainstem Nuclei (Harvard Ascending Arousal Network)** asdf

**Brainstem Filler (Shen268)** asdf

Assembling CANlab2025 from openCANLab2025

CANLab2025 is assembled by substitution of regions from the Harvard Ascending Arousal Network atlas and the nucleus tractus solitarius from the Levinson-Bari Limbic Brainstem atlas with regions from the Bianciardi v0.9 brainstem atlas. Substitution requires matlab (tested on versions r2019a and later) and a POSIX compliant \*nix environment with a minimum of 32G of RAM and 32G of scratch space on disk. Substituted regions are all indexed last in openCANLab2025, and Bianciardi regions are appended in such a way that all regions shared by openCANLab2025 and CANLab2025 also share the same indices across atlases.

## **Participants**

[consolidate discussion of participant counts from other sections including: thalamic segmentation]

## Task GLM

[describe first level GLM designs here used in evaluations]

## Evaluation

**Surface to volume projection** [Criteria should be described here]

## **Brainstem labels** [PET tracer comparisons go here]

## Results

An overview of the CANLab2025 atlas is presented in figure 1.

## Overview of parcellations

Each structure is subdivided into multiple nested levels of parcels. Here we will present each gross structure and nested parcellations thereof. There are four levels of nesting (Figure 2). Level 1 is optimized for signal attribution and reverse inference, but many structures are likely too small and inconsistently localized for robust use in many applications. For instance, the typical T2\* EPI imaging sequences sample the brain with 3mm isotropic voxels, and the point spread function of the BOLD signal at 3T has a full width half maximum of 3mm [citation needed], corresponding to an effective spatial resolution of 27mm<sup>3</sup>, but in a forced choice parcellation scheme 21 of our finest regions have volumes smaller than this. These regions may be useful for reverse inference, since their probability maps extend over a larger region of space, but in most of that space neighboring structures are more probable and would be selected instead by deterministic parcellation schemes. Level 2 provides an alternative, designed for tractography, deterministic parcellation and region of interest analysis. Level 3 offers a coarser alternative to level 2 possibly better suited to legacy data and registration techniques or computationally demanding applications. Level 4 provides a natural grouping of finer levels of granularity (e.g. Caudate, Putamen, Hippocampal formation, cerebellar cortex, etc.) to facilitate targeted analysis of large scale structures. For cortex

and cerebellum, no extremely small parcels exist, and therefore levels 1 and 2 are redundant. Parcellations at each scale for each large scale structure are detailed below.

**Cortex** Probabilistic labels (Figure ??); Granularities (Figure 3) [compare with Huang et al. 2022 Brain Structure and Function and Horn et al 2016]

**Thalamus** [this requires some attention to the habenula and its relationship with neighboring structures. Commentary is also needed in differences between 1mm and 2mm versions of the atlas, in particular, at 2mm there are no midline structures (where do they go? Are they subsumed by rostral intralaminar [rIL] regiois?)]

**Basal Ganglia** The basal ganglia in CANLab2025 are one of two categories of structures where labels differ in volumetric and grayordinate atlases. The basal ganglia are constituted by parcels from Tian, Cartmell and CIT atlases. Although Tian is derived from the same data used to define the grayordinate space (HCP), and therefore abides by the grayordinate boundaries perfectly, CIT and Cartmell do not. To better accommodate ventral striatal regions derived from these atlases the volumetric parcels were allowed to exceed the CIFTI boundaries slightly, which is most visible when comparing the left (red) and right (green) ventral striatal parcels in Figure 6 with the grayordinate parcel boundaries (black outlines). This introduces slight differences between volumetric and CIFTI versions of CANLab2025, since these areas outside of the grayordinate boundaries are therefore absent in the latter. Notably, the divisions between accumbens in the putamen and accumbens/caudate are also not identical to the grayordinate structures, which limits the utility of grayordinate structural labels when using this atlas. For instance, using connectome workbench to extract the “ACCUMBENS\_LEFT” structure will select only a subset of the CANLab2025 accumbens, while trying to extract “CAUDATE\_LEFT” will result in a mixture of caudate and ventral striatum parcels. This inconsistency across atlases is consistent with the absence of clear criteria for delineating the transitions between these regions (S. N. Haber & Knutson, 2010; Tian et al., 2020), but we believe that functional (Tian et al., 2020) and tractography based criteria (Cartmell et al., 2019) should take precedence over the gray matter contrast based criteria according to which the grayordinate labels were defined [situation needed].

**Hypothalamus** After the basal ganglia, the hypothalamus in CANLab2025 is the only additional structure=s where labels differ in volumetric and grayordinate atlases. Here we include the optic nuclei anterior to the hypothalamus in our definition since these are all part of the same source atlas (Billot et al.,

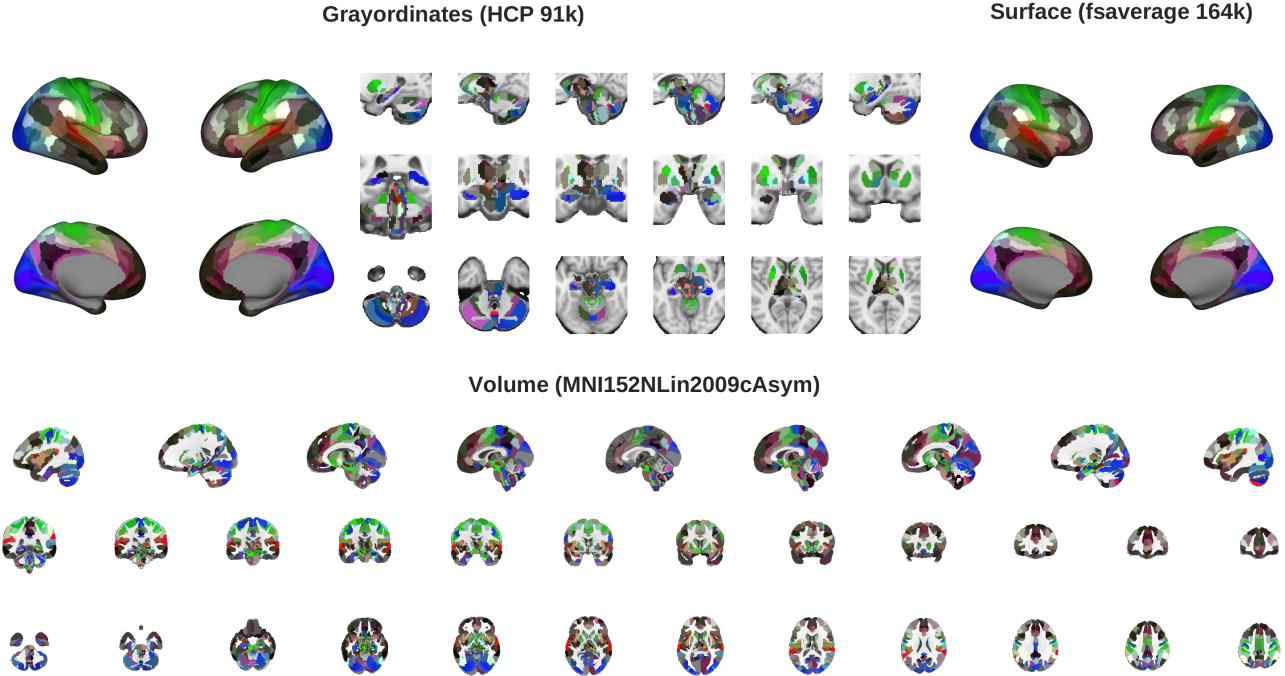


**Figure 1: CANLab2025, at its most granular, illustrated in multiple spaces.** 601 parcels are shown, 358 cortical, 243 subcortical. Grayordinates are shown on the S1200 HCP 91k inflated surface or a MNI152NLin6Asym template underlay. Surface labels are shown on the fsaverage 164k inflated surface. Meanwhile, volumetric plots use a MNI152NLin2009cAsym underlay. The tight correspondence between labels, surfaces and underlays qualitatively illustrates the precision and versatility of our labels. Colors adapted from (Glasser et al., 2016).

2020). These nuclei are quite small, but of particular interest since they process visual stimuli and project to thalamic areas that are highly distinct from the homeostatic function and limbic, prefrontal and brainstem projections that innervate the rest of the hypothalamus. Masking them to restrict the hypothalamus to the HCP 91k grayordinate boundaries would erode a large percentage of these optic nuclei (Figure 8), therefore we retain these despite the incongruity it introduces between CIFTI and NIFTI versions of CANLab2025. These regions are the first to go though as we downsample our parcellation and they become subsumed by the their larger neighbors (Figure 7), so the scope of the incongruity is limited to the finest parcellation (level 1).

**Amygdala/Hippocampus** We describe the medial temporal lobe structures jointly because the boundaries between amygdala and hippocampus are poorly defined, so our boundaries are not guaranteed to align with those of the HCP 91k grayordinate parcels to which we project our atlas. Nevertheless, comparison of our level 4 (coarsest) labels, which subdivide the medial temporal lobe into amygdala and hippocampal formation, shows very close correspondence with the HCP 91k hippocampal and amygdala grayordinate structures.

**Cerebellum** The cerebellar atlas is derived from the SUIT atlas (Diedrichsen et al., 2009). This parcellation was already quite coarse (Figure 2), distinguishing cerebellar lobules and

segments of the vermis, so it was not downsampled further except for levels 3 and 4 of granularity (the coarsest two; Figure 11).

**Brainstem** In the case of the brainstem we have gray matter and white matter intermingled, with poorly defined boundaries, and available digital atlases are incomplete. As a result we define the nuclei for which definitions are available but also introduce filler labels for residual voxels with descriptive labels (e.g. left ventral rostral pons). For display purposes we omit these latter regions. Additionally, the brainstem is where openCANLab2025 and CANLab2025 diverge due to the inclusion of regions from the Bianciardi brainstem atlas in the latter, which are not openly licensed. Thus, we focus here on highlighting these differences.

[This needs a plot of the level 2 PAG vs. the level 1 PAG + CnF]

[compare locus coeruleus in Bianciardi and Levinson-Bari. Justify use of Levinson-Bari as similar enough and open]

[Could include neurotransmitter maps here potentially]

## Discussion

[The difference in size of regions between cortex and cerebellum vs. brainstem, thalamus and BG should maybe not be surprising. The cortex and cerebellum are the two brain areas that had to fold in on themselves to be able to fit inside

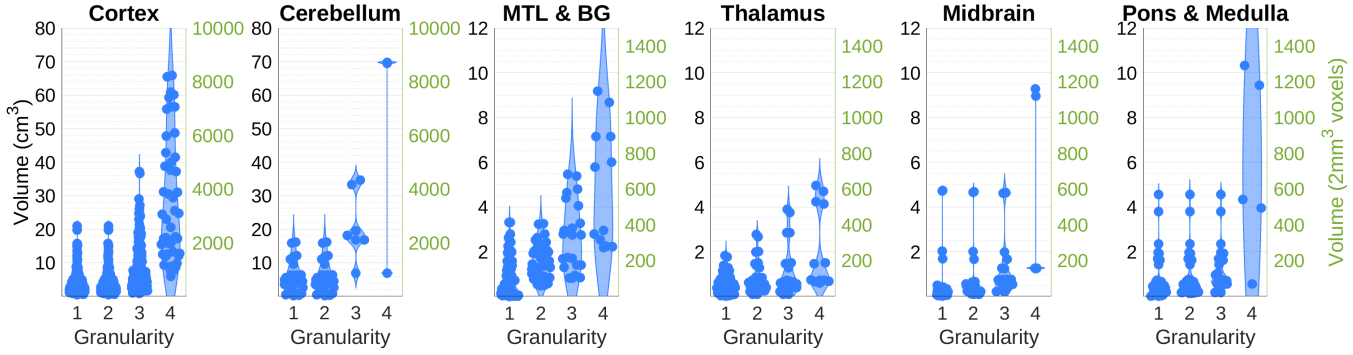


**Figure 2: Four nested parcellation are available which vary in granularity from fine to coarse to help balance between the demands of different use cases.** Some regions are difficult to localize at the resolution of popular registration templates ( $2\text{mm}^3$  isotropic, right axes). Fine scale regions are merged with functional or structurally related neighbors to produce coarser granularities that may be more practical in some applications. MTL: medial temporal lobe; BG: basal ganglia.

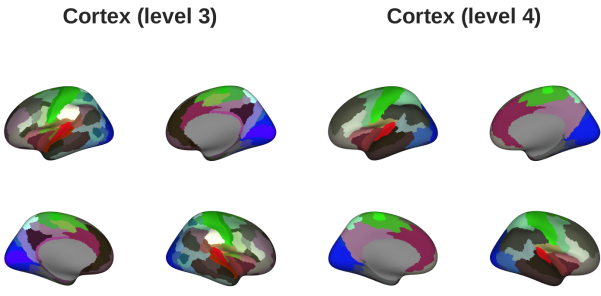


**Figure 3: CANLab2025 cortical parcels: coarser subdivisions.** The finest granularity of cortical parcels (level 1) was shown in Figure 1, but two coarser parcellations are also available (level 3 and level 4). Levels 2 is generally a downsampled version of level 1 that is more suitable for practical use as a priori ROIs, but in the case of the cortical parcels all regions were already large enough for such use, so no additional downsampling was used at level 2, and it is redundant with level 1.

the skull. There's clearly something distinct about the scale at which they operate.]

**Cortex** Our volumetric cortical parcellation accounts for the idiosyncratic folding across individuals, but does not account for idiosyncrasies in functional and structural topographies reported by Glasser et al. It seems unlikely at this point that Glasser et al. will ever release their idiosyncratic subject specific parcellations or the structural and functional feature based parcel classifiers they used to generate them, but their data is available and this leaves the door open for further refinements of this parcellation. Using the publicly available HCP data it would be possible to characterize each parcel in terms of population average multimodal features and use those to produce subject specific parcellations based on a nearest neighbor classification scheme or some similar strategy. It would be straightforward to combine such subject spe-

cific parcellations into probabilistic labels in surface space. Reprojection from surface to volume space would produce volumetric probabilistic labels that account for both area identity and its idiosyncratic embedding in 3D space. For now however our probabilities only account for idiosyncrasies in cortical folding, and should be used accordingly.

**Thalamus** [look up your iglesias atlas git repo README. There's a long section on the 'veracity of the atlas' with issues worth discussing]

**Caudate/Putamen** [Address issues with using functional connectivity gradients as a criterion]

**Brainstem** [discuss how brainstem is incomplete and likely to continue to develop. Can give the RVM as an example region we tried to include but couldn't, and describe why we couldn't. Discuss licensing restrictions and alternative atlases (or the lack thereof). Discuss how localization is a problem here and how probabilistic labels should be combined with expert knowledge to correctly attribute signals to structures. Can use the olfactory complex as an example since SOC and ION are hard to distinguish. LC might be even better.]

**Variations across file formats** [discuss the slight differences in the ventral striatum and hypothalamus, the absence of deep cerebellar nuclei, and the need for an update to the HCP 91k grayordinate template. Discuss surface representations of the cerebellum as well, and speculate on future extensions of the atlas that take advantage of superior grayordinate templates.]

**Credit attribution** The efforts involved in assembling this atlas were substantial, but do not compare to those involved in generating the atlases we've built CANLab2025 from. We ask that those using CANLab2025 give credit where credit is due. Appropriate references are listed in Table 1 for precisely this reason. This paper should be cited merely to the extent necessary for documenting our modifications to this prior work.

Limitations of histology? (registration issues, tissue distor-

tion)

usefulness in neurosurgery?

what about still unlabeled voxels? Ideally we'd have a structural label for every single voxel. We still need white matter structures for this.

## Data Availability

CANLab2025 and all constituent atlases are available online through our github repository: [https://github.com/canlab/Neuroimaging\\_Pattern\\_Masks/](https://github.com/canlab/Neuroimaging_Pattern_Masks/). For further details regarding (open)CANLab2025 specifically please refer to [https://github.com/canlab/Neuroimaging\\_Pattern\\_Masks/tree/master/Atlases\\_and\\_parcellations/2025\\_CANLab\\_atlas/README.md](https://github.com/canlab/Neuroimaging_Pattern_Masks/tree/master/Atlases_and_parcellations/2025_CANLab_atlas/README.md). All subject specific cortical projections used for registration fusion are available at [https://figshare.com/articles/dataset/2016\\_Glasser\\_MMP1\\_0\\_Cortical\\_Atlases/24431146](https://figshare.com/articles/dataset/2016_Glasser_MMP1_0_Cortical_Atlases/24431146).

## Acknowledgements

We thank Ye Tian and Andrew Zalesky for sharing subject level segmentations of the basal ganglia, Henry Tregidgo and Juan Eugenio Iglesias for help with multimodal Bayesian segmentation of thalamic subnuclei, Philip A Kragel for suggesting the use of the CIT amygdala parcellation and providing subject specific PAG segmentations from which probabilities could be derived, and Mijin Kwon for guidance on optimal assignment of glasser parcels to the classic granular, agranular and dysgranular subdivisions of the insula. We additionally thank Michael Sun for working with CANLab2025 and providing valuable feedback on usability and bugs.

This research was funded by NIBIB R01EB026549.

## References

- Amunts, K., Kedo, O., Kindler, M., Pieperhoff, P., Mohlberg, H., Shah, N. J., ... Zilles, K. (2005, 12). Cytoarchitectonic mapping of the human amygdala, hippocampal region and entorhinal cortex: intersubject variability and probability maps. *Anatomy and embryology*, 210, 343-52. Retrieved from <http://www.ncbi.nlm.nih.gov/pubmed/16208455> doi: 10.1007/s00429-005-0025-5
- Amunts, K., Mohlberg, H., Bludau, S., & Zilles, K. (2020, 8). Julich-brain: A 3d probabilistic atlas of the human brain's cytoarchitecture. *Science*, 369, 988-992. Retrieved from <https://www.sciencemag.org/lookup/doi/10.1126/science.abb4588> doi: 10.1126/science.abb4588
- Bianciardi, M., Strong, C., Toschi, N., Edlow, B. L., Fischl, B., Brown, E. N., ... Wald, L. L. (2018, 4). A probabilistic template of human mesopontine tegmental nuclei from in vivo 7 t mri. *NeuroImage*, 170, 222-230. doi: 10.1016/j.neuroimage.2017.04.070
- Bianciardi, M., Toschi, N., Edlow, B. L., Eichner, C., Setsompop, K., Polimeni, J. R., ... Wald, L. L. (2015, 12). Toward an in vivo neuroimaging template of human brainstem nuclei of the ascending arousal, autonomic, and motor systems. *Brain Connectivity*, 5, 597-607. doi: 10.1089/brain.2015.0347
- Bianciardi, M., Toschi, N., Eichner, C., Polimeni, J. R., Setsompop, K., Brown, E. N., ... Wald, L. L. (2016, 6). In vivo functional connectome of human brainstem nuclei of the ascending arousal, autonomic, and motor systems by high spatial resolution 7-tesla fmri. *Magnetic Resonance Materials in Physics, Biology and Medicine*, 29, 451-462. doi: 10.1007/s10334-016-0546-3
- Billot, B., Bocchetta, M., Todd, E., Dalca, A. V., Rohrer, J. D., & Iglesias, J. E. (2020, 12). Automated segmentation of the hypothalamus and associated subunits in brain mri. *NeuroImage*, 223. doi: 10.1016/j.neuroimage.2020.117287
- Botvinik-Nezer, R., Petre, B., Ceko, M., Lindquist, M. A., Friedman, N. P., & Wager, T. D. (2023). Placebo treatment affects brain systems related to affective and cognitive processes, but not nociceptive pain. *bioRxiv*. Retrieved from <https://www.biorxiv.org/content/early/2023/09/30/2023.09.21.558825> doi: 10.1101/2023.09.21.558825
- Cartmell, S. C., Tian, Q., Thio, B. J., Leuze, C., Ye, L., Williams, N. R., ... Halpern, C. H. (2019, 9). Multimodal characterization of the human nucleus accumbens. *NeuroImage*, 198, 137-149. doi: 10.1016/j.neuroimage.2019.05.019
- Coalson, T. S., Essen, D. C. V., & Glasser, M. F. (2018, 7). The impact of traditional neuroimaging methods on the spatial localization of cortical areas. *Proceedings of the National Academy of Sciences*, 115. Retrieved from <https://pnas.org/doi/full/10.1073/pnas.1801582115> (Illustration of the relative advantages of surface based vs. volumetric alignment. Good citation to motivate use of cortical surface models, but also useful for qualifying cerebellar alignment results, where a surface exists but we don't have a model for it yet.) doi: 10.1073/pnas.1801582115
- Desikan, R. S., Ségonne, F., Fischl, B., Quinn, B. T., Dickerson, B. C., Blacker, D., ... Killiany, R. J. (2006). An automated labeling system for subdividing the human cerebral cortex on mri scans into gyral based regions of interest. *NeuroImage*, 31(3), 968-980. Retrieved from <https://www.sciencedirect.com/science/article/pii/S1053811906000437> doi: <https://doi.org/10.1016/j.neuroimage.2006.01.021>
- Destrieux, C., Fischl, B., Dale, A., & Halgren, E. (2010). Automatic parcellation of human cortical gyri and sulci using standard anatomical nomenclature. *NeuroImage*, 53(1), 1-15. Retrieved from <https://www.sciencedirect.com/science/article/pii/S1053811910008542> doi: <https://doi.org/10.1016/j.neuroimage.2010.06.010>
- Diedrichsen, J., Balsters, J. H., Flavell, J., Cussans, E., & Ramnani, N. (2009, 5). A probabilistic mr atlas of the human cerebellum. *NeuroImage*, 46, 39-46. doi: 10.1016/j.neuroimage.2009.01.045
- Edlow, B. L., Olchanyi, M., Freeman, H. J., Li, J., Maffei,

- C., Snider, S. B., ... Kinney, H. C. (2023). Sustaining wakefulness sustaining wakefulness: Brainstem connectivity in human consciousness. *bioRxiv*. Retrieved from <https://doi.org/10.1101/2023.07.13.548265> doi: 10.1101/2023.07.13.548265
- Edlow, B. L., Takahashi, E., Wu, O., Benner, T., Dai, G., Bu, L., ... Folkerth, R. D. (2012, 6). Neuroanatomic connectivity of the human ascending arousal system critical to consciousness and its disorders. *Journal of Neuropathology & Experimental Neurology*, 71, 531-546. Retrieved from <https://academic.oup.com/jnen/article-lookup/doi/10.1097/NEN.0b013e3182588293> doi: 10.1097/NEN.0b013e3182588293
- Essen, D. C. V., Smith, S. M., Barch, D. M., Behrens, T. E., Yacoub, E., & Ugurbil, K. (2013, 10). The wu-minn human connectome project: An overview. *NeuroImage*, 80, 62-79. doi: 10.1016/j.neuroimage.2013.05.041
- Fischl, B., Salat, D. H., Busa, E., Albert, M., Dieterich, M., Haselgrave, C., ... Dale, A. M. (2002). Whole brain segmentation: Automated labeling of neuroanatomical structures in the human brain. *Neuron*, 33(3), 341-355. Retrieved from <https://www.sciencedirect.com/science/article/pii/S089662730200569X> doi: [https://doi.org/10.1016/S0896-6273\(02\)00569-X](https://doi.org/10.1016/S0896-6273(02)00569-X)
- García-Gomar, M. G., Strong, C., Toschi, N., Singh, K., Rosen, B. R., Wald, L. L., & Bianciardi, M. (2019). In vivo probabilistic structural atlas of the inferior and superior colliculi, medial and lateral geniculate nuclei and superior olive complex in humans based on 7 tesla mri. *Frontiers in Genetics*, 10. doi: 10.3389/fnins.2019.00764
- Glasser, M. F., Coalson, T. S., Robinson, E. C., Hacker, C. D., Harwell, J., Yacoub, E., ... Essen, D. C. V. (2016). A multimodal parcellation of human cerebral cortex. *Nature*, 536, 171-8. Retrieved from <http://www.ncbi.nlm.nih.gov/pubmed/27437579> doi: 10.1038/nature18933
- Glasser, M. F., Sotiroopoulos, S. N., Wilson, J. A., Coalson, T. S., Fischl, B., Andersson, J. L., ... Jenkinson, M. (2013, 10). The minimal preprocessing pipelines for the human connectome project. *NeuroImage*, 80, 105-24. Retrieved from <http://www.ncbi.nlm.nih.gov/pubmed/23668970> doi: 10.1016/j.neuroimage.2013.04.127
- Haber, S., & Watson, S. (1985, 4). The comparative distribution of enkephalin, dynorphin and substance p in the human globus pallidus and basal forebrain. *Neuroscience*, 14, 1011-1024. Retrieved from <https://linkinghub.elsevier.com/retrieve/pii/0306452285902726> doi: 10.1016/0306-4522(85)90272-6
- Haber, S. N., & Knutson, B. (2010, 1). *The reward circuit: Linking primate anatomy and human imaging* (Vol. 35). doi: 10.1038/npp.2009.129
- Holmes, C. J., Hoge, R., Collins, L., Woods, R., Toga, A. W., & Evans, A. C. (1998). Enhancement of MR images using registration for signal averaging. *J. Comput. Assist. Tomogr.*, 22(2), 324–333.
- Iglesias, J. E., Insausti, R., Lerma-Usabiaga, G., Bocchetta, M., Leemput, K. V., Greve, D. N., ... Paz-Alonso, P. M. (2018, 12). A probabilistic atlas of the human thalamic nuclei combining ex vivo mri and histology. *NeuroImage*, 183, 314-326. doi: 10.1016/j.neuroimage.2018.08.012
- Klein, A., & Tourville, J. (2012). 101 labeled brain images and a consistent human cortical labeling protocol. *Frontiers in Neuroscience*, 6. Retrieved from <https://www.frontiersin.org/journals/neuroscience/articles/10.3389/fnins.2012.00171> doi: 10.3389/fnins.2012.00171
- Kragel, P. A., Bianciardi, M., Hartley, L., Matthewson, G., Choi, J. K., Quigley, K. S., ... Satpute, A. B. (2019, 7). Functional involvement of human periaqueductal gray and other midbrain nuclei in cognitive control. *Journal of Neuroscience*, 39, 6180-6189. doi: 10.1523/JNEUROSCI.2043-18.2019
- Leung, B. K., & Balleine, B. W. (2015). Ventral pallidal projections to mediodorsal thalamus and ventral tegmental area play distinct roles in outcome-specific pavlovian-instrumental transfer. *Journal of Neuroscience*, 35, 4953-4964. doi: 10.1523/JNEUROSCI.4837-14.2015
- Levinson, S., Miller, M., Iftekhar, A., Justo, M., Arriola, D., Wei, W., ... Bari, A. A. (2023, 1). A structural connectivity atlas of limbic brainstem nuclei. *Frontiers in Neuroimaging*, 1. Retrieved from <https://www.frontiersin.org/articles/10.3389/fnimg.2022.1009399/full> doi: 10.3389/fnimg.2022.1009399
- Losin, E. A. R., Woo, C.-W., Medina, N. A., Andrews-Hanna, J. R., Eisenbarth, H., & Wager, T. D. (2020, 5). Neural and sociocultural mediators of ethnic differences in pain. *Nature Human Behaviour*, 4, 517-530. Retrieved from <http://dx.doi.org/10.1038/s41562-020-0819-8> doi: 10.1038/s41562-020-0819-8
- Mai, J., Paxinos, G., & Voss, T. (2008). *Atlas of the human brain*. Elsevier Science. Retrieved from <https://books.google.com/books?id=CWghAQAAQAAJ>
- Pauli, W. M., Nili, A. N., & Tyszka, J. M. (2018, 4). Data descriptor: A high-resolution probabilistic in vivo atlas of human subcortical brain nuclei. *Scientific Data*, 5. doi: 10.1038/sdata.2018.63
- Reiner, A., Medina, L., & Haber, S. N. (1999). The distribution of dynorphinergic terminals in striatal target regions in comparison to the distribution of substance p-containing and enkephalinergic terminals in monkeys and humans. *Neuroscience*, 88, 775-793. (Cited to support inclusion of the ventral pallidum in the internal rather than external segment of CANLab2024 coarse parcellations)
- Shen, X., Tokoglu, F., Papademetris, X., & Constable, R. T. (2013, 11). Groupwise whole-brain parcellation from resting-state fmri data for network node identification. *NeuroImage*, 82, 403-415. doi: 10.1016/j.neuroimage.2013.05.081
- Singh, K., Indovina, I., Augustinack, J. C., Nestor, K., García-

Gomar, M. G., Staab, J. P., & Bianciardi, M. (2020, 1). Probabilistic template of the lateral parabrachial nucleus, medial parabrachial nucleus, vestibular nuclei complex, and medullary viscero-sensory-motor nuclei complex in living humans from 7 tesla mri. *Frontiers in Neuroscience*, 13. doi: 10.3389/fnins.2019.01425

Talairach, J., & Tournoux, P. (1988). *Co-planar stereotaxic atlas of the human brain: 3-dimensional proportional system : an approach to cerebral imaging*. G. Thieme. Retrieved from <https://books.google.com/books?id=pYFiQgAACAAJ>

Tian, Y., Margulies, D. S., Breakspear, M., & Zalesky, A. (2020, 11). Topographic organization of the human subcortex unveiled with functional connectivity gradients. *Nature Neuroscience*, 23, 1421-1432. doi: 10.1038/s41593-020-00711-6

Tregidgo, H. F., Soskic, S., Althonayan, J., Maffei, C., Leemput, K. V., Golland, P., ... Iglesias, J. E. (2023, 7). Accurate bayesian segmentation of thalamic nuclei using diffusion mri and an improved histological atlas. *NeuroImage*, 274. doi: 10.1016/j.neuroimage.2023.120129

Tregidgo, H. F. J., Soskic, S., Olchanyi, M. D., Althonayan, J., Billot, B., Maffei, C., ... Iglesias, J. E. (2023). Domain-agnostic segmentation of thalamic nuclei from joint structural and diffusion mri. In H. Greenspan et al. (Eds.), *Medical image computing and computer assisted intervention – miccai 2023* (pp. 247–257). Cham: Springer Nature Switzerland.

Tyszka, J. M., & Pauli, W. M. (2016, 11). In vivo delineation of subdivisions of the human amygdaloid complex in a high-resolution group template. *Human Brain Mapping*, 37, 3979-3998. doi: 10.1002/hbm.23289

Wu, J., Ngo, G. H., Greve, D., Li, J., He, T., Fischl, B., ... Yeo, B. T. (2018, 9). Accurate nonlinear mapping between mni volumetric and freesurfer surface coordinate systems. *Human Brain Mapping*, 39, 3793-3808. doi: 10.1002/hbm.24213

Xue, A., Kong, R., Yang, Q., Eldaief, M. C., Angeli, P. A., DiNicola, L. M., ... Yeo, B. T. T. (2021). The detailed organization of the human cerebellum estimated by intrinsic functional connectivity within the individual. *Journal of Neurophysiology*, 125(2), 358-384. Retrieved from <https://doi.org/10.1152/jn.00561.2020> (PMID: 33427596) doi: 10.1152/jn.00561.2020

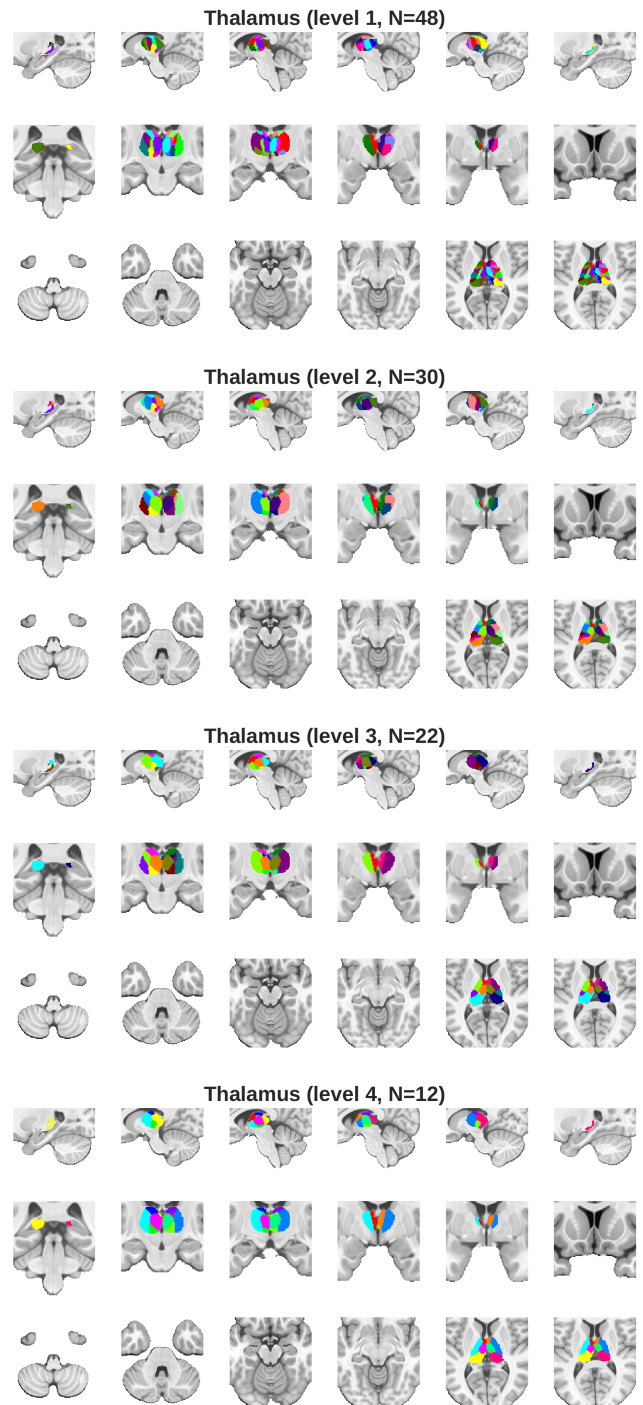


Figure 4: CANLab2025 thalamic parcels

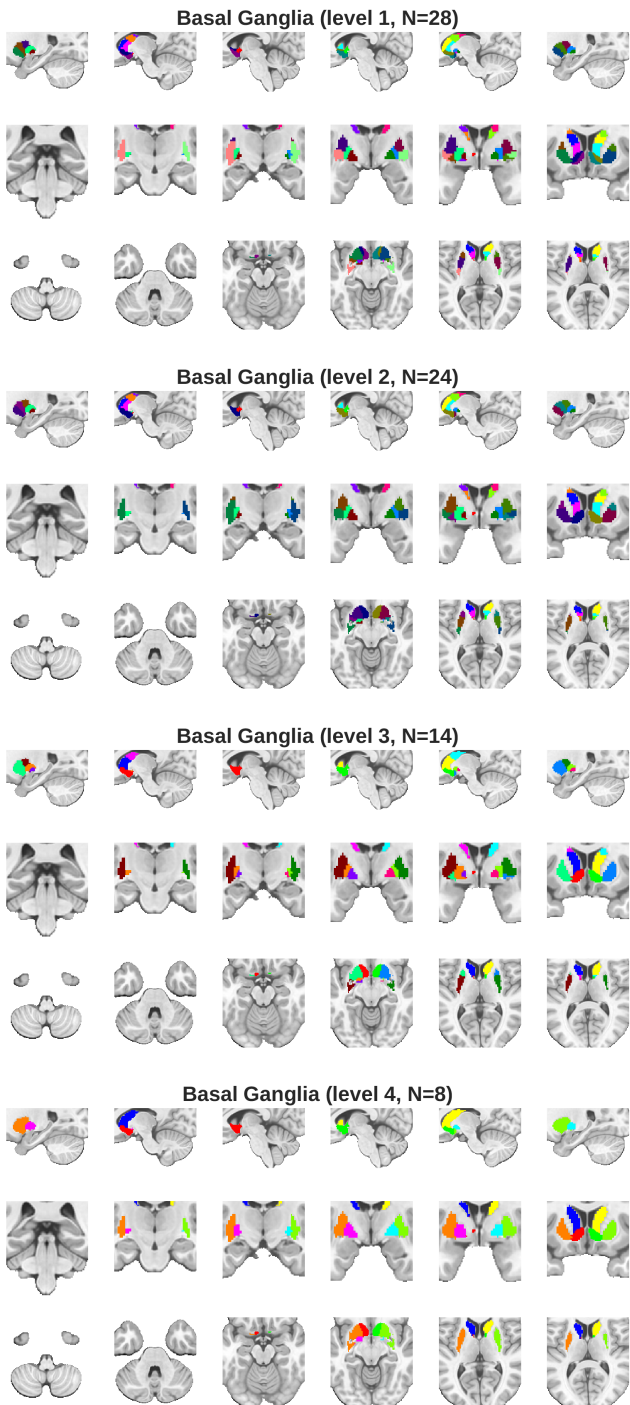
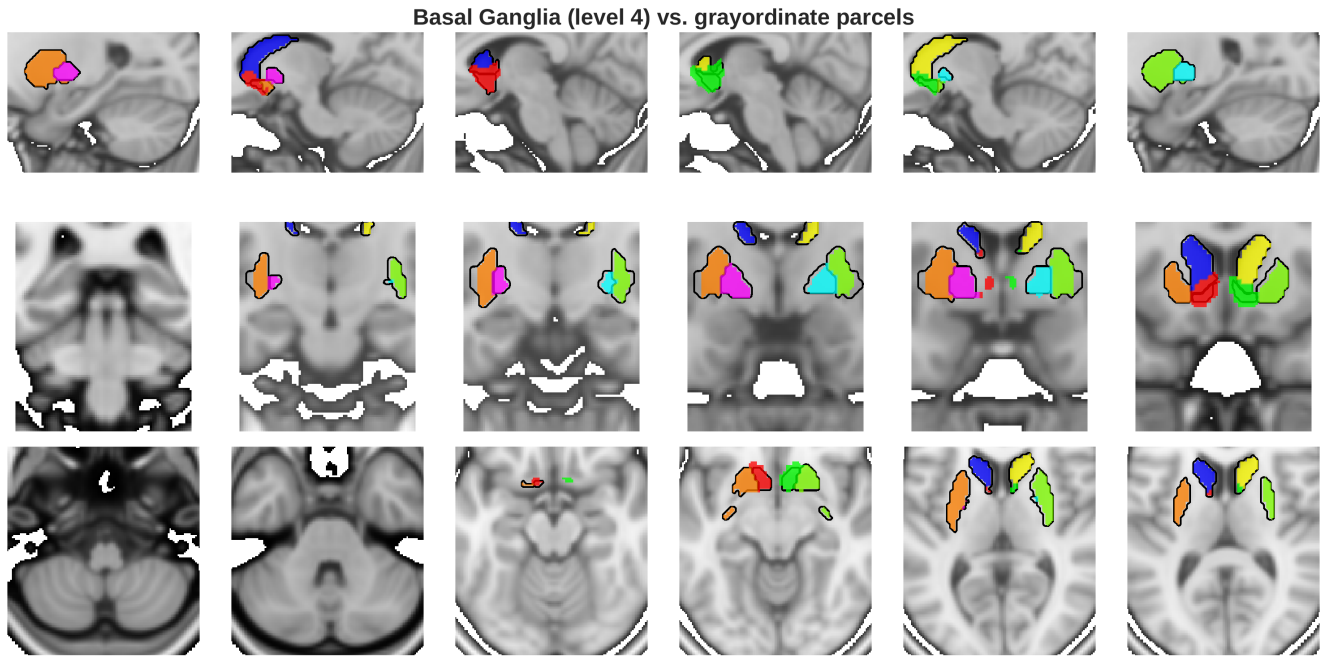
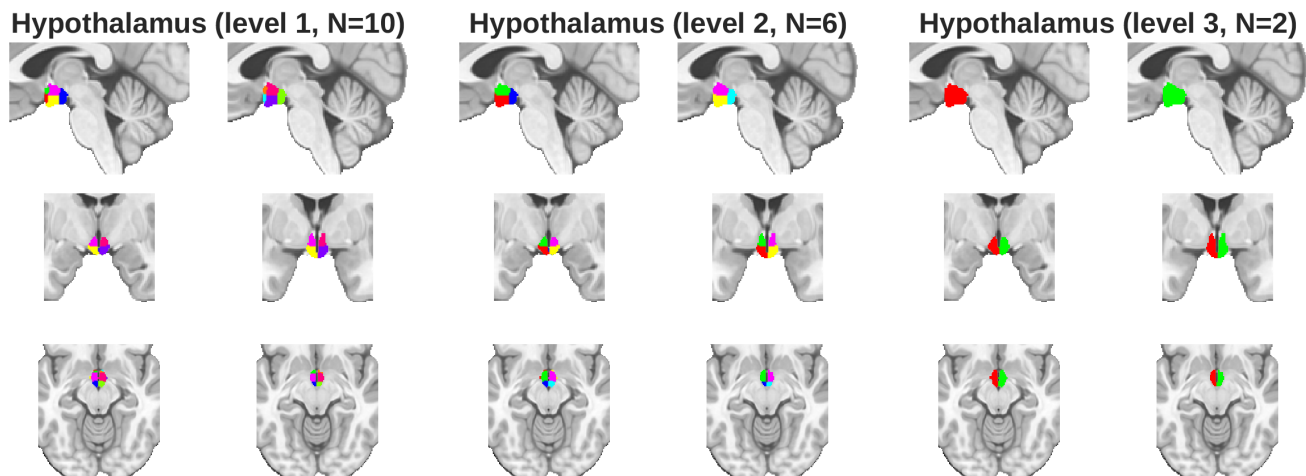


Figure 5: CANLab2025 basal ganglia parcels



**Figure 6: CANLab2025 basal ganglia parcels differ from CIFTI grayordinate structural boundaries.** Colored outlines indicate the coarsest level of parcellation for the basal ganglia, and trace the boundaries of classic gross nuclei except for the ventral striatum which includes the nucleus accumbens as well as portions of the extended amygdala. Black lines illustrate the boundaries of corresponding structures in HCP 91k grayordinate space. CANLab2025 boundaries in the ventral striatum exceed those of the grayordinate structures, therefore grayordinate versions of the atlas will include slightly eroded ventral striatal regions relative to volumetric atlases. Meanwhile, the most lateral portions of the putamen are excluded from our atlas parcellations in all spaces despite inclusion within the grayordinate boundaries. This is to avoid redundancy with surface insular vertices with which they often overlap. Underlay: MNI152NLin6Asym T1 2mm template, used by HCP 91k grayordinates.



**Figure 7: CANLab2025 hypothalamic parcels.** The optic nuclei are merged with anterior hypothalamic nuclei at level 2 while keeping the posterior mammillary bodies separate. All nuclei are merged at level 3. The fourth level of granularity is identical to the third (not shown).

## Figure 8: CANLab2025 vs. HCP 91k

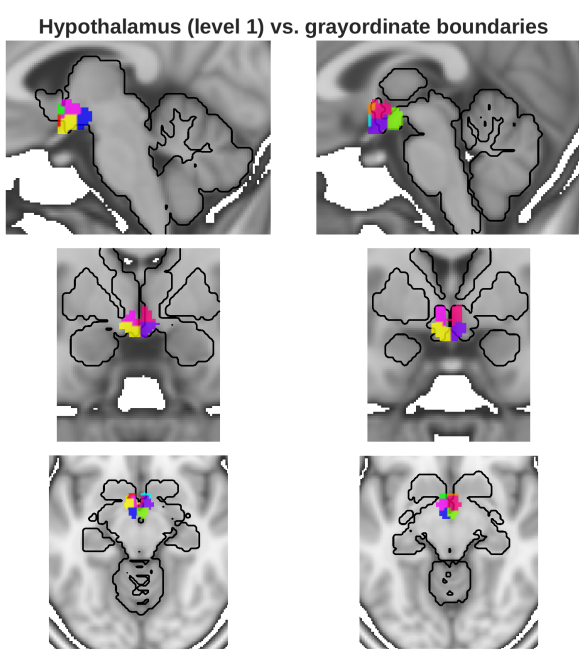


**Figure 8: CANLab2025 hypothalamus parcels exceed HCP 91k grayordinate structural boundaries.** Colored outlines indicate the finest level of parcellation for the hypothalamus. Black lines illustrate the boundaries of HCP 91k grayordinate space. Although the boundaries coincide well enough for most nuclei, masking the hypothalamus with grayordinate boundaries would have dramatically affected the anterior optic nuclei. Underlay: MNI152NLin6Asym T1 2mm template, used by HCP 91k grayordinates.

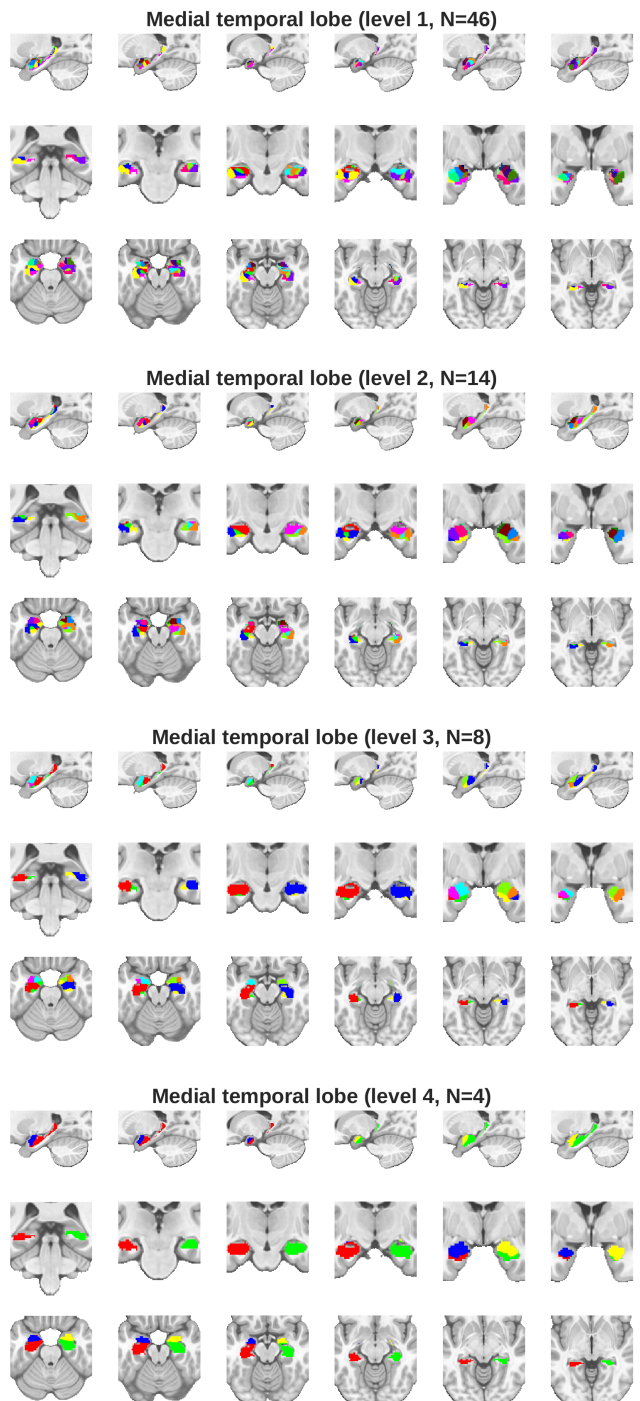


**Figure 9: CANLab2025 Medial temporal lobe parcels.** At level 1 CANLab2025 distinguishes between intercalated nuclei of the amygdala, the central and median nuclei of the amygdala, and between CA2 and CA3 of the hippocampus. At level 2 these distinctions are collapsed and the intercalated nuclei are subsumed by their nearest neighbors while central and median nuclei and CA2 and CA3 are merged. At level 3 the amygdala is subdivided into basolateral, lateral and centromedian subdivisions, while the hippocampal formation is merely subdivided into hippocampus proper and subiculum. Level 4 subdivides the amygdala from the hippocampus.

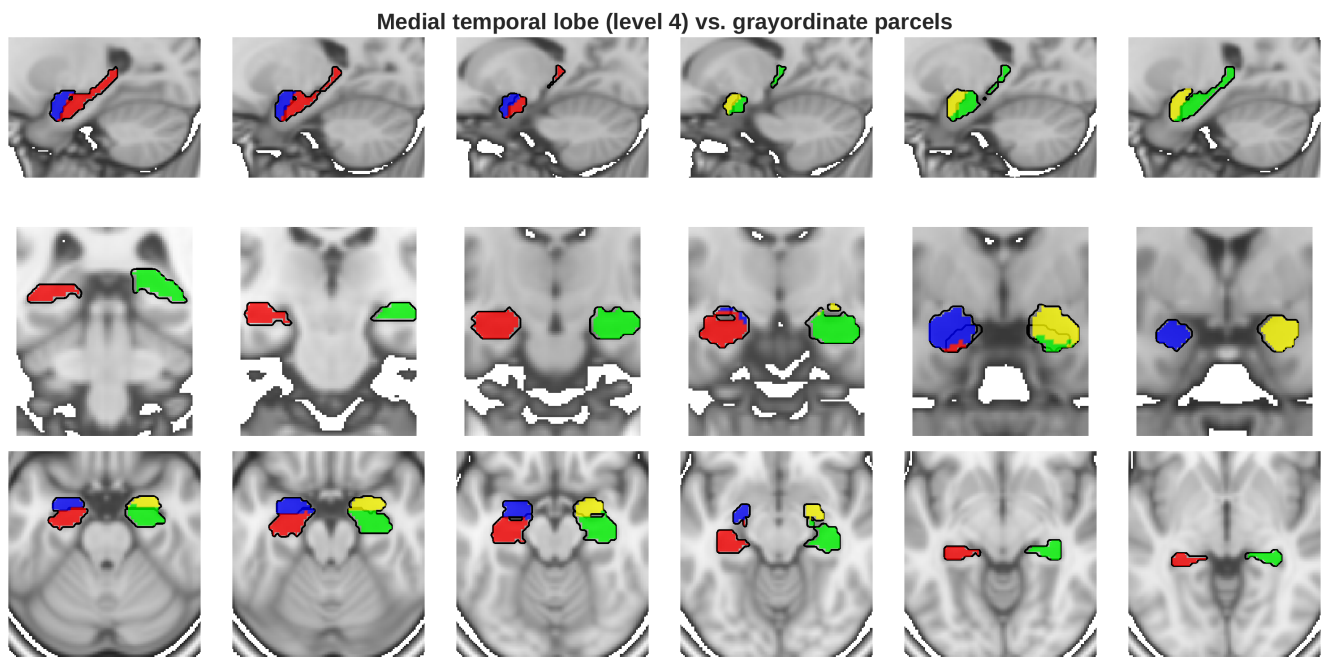


**Figure 10: CANLab2025 medial temporal lobe parcels align well with HCP 91k grayordinate structural boundaries.** Colored outlines indicate the coarsest level of parcellation for the medial temporal lobe structures. Black lines illustrate the boundaries of HCP 91k grayordinate space. Underlay: MNI152NLin6Asym T1 2mm template, used by HCP 91k grayordinates.

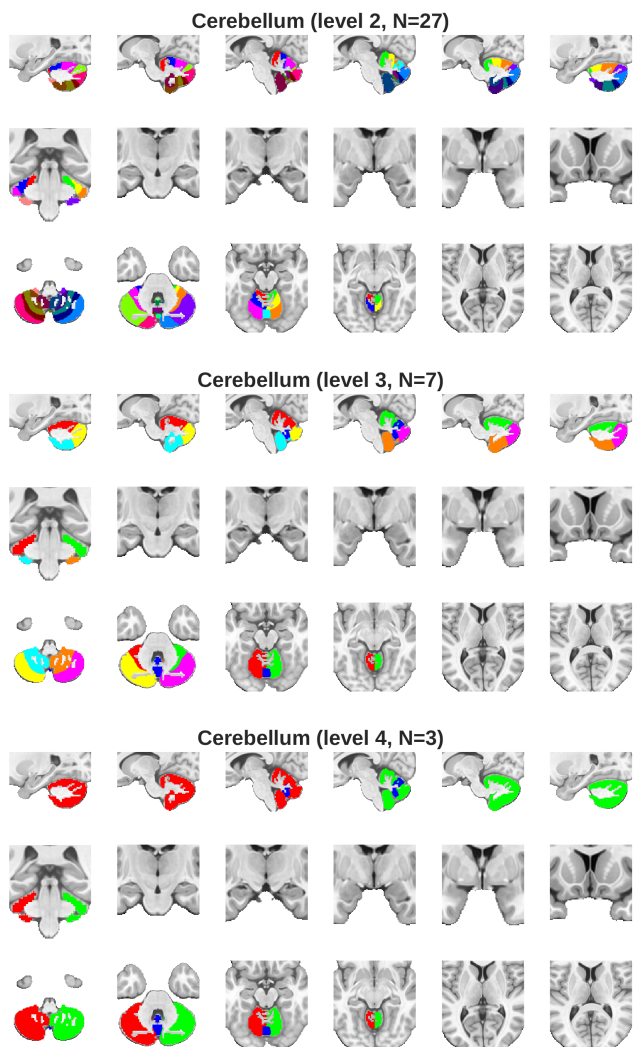
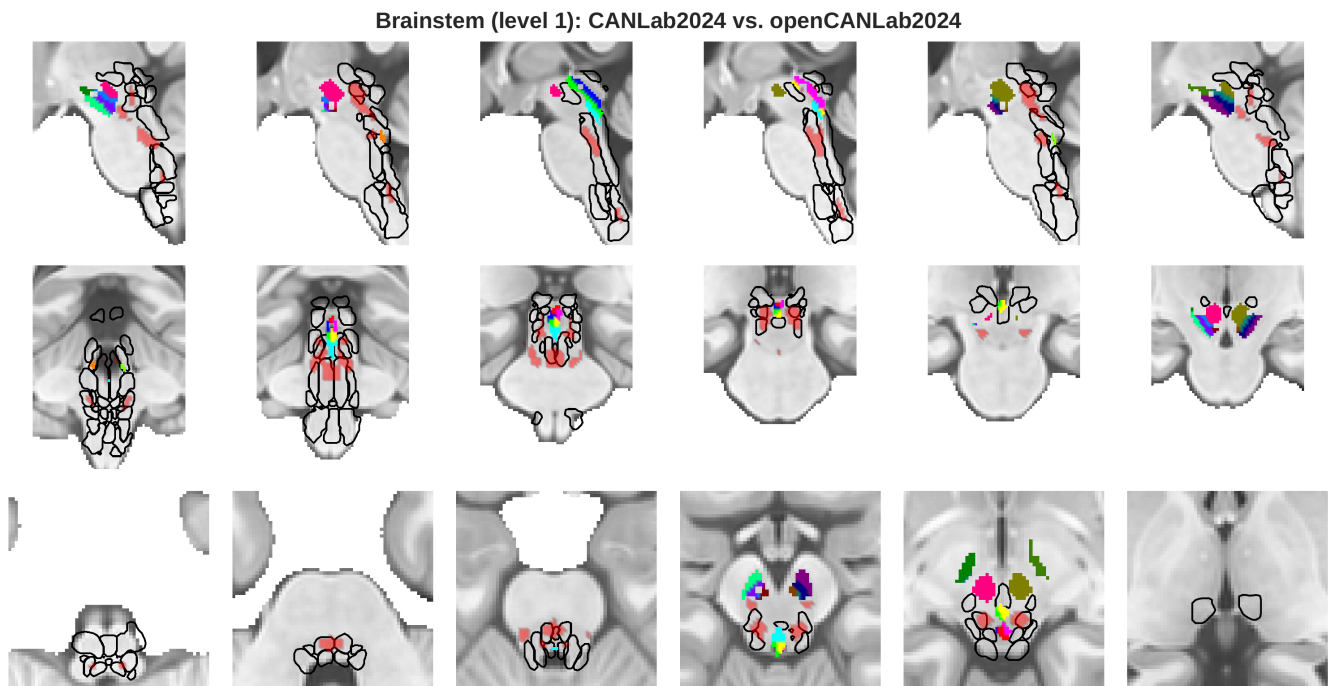
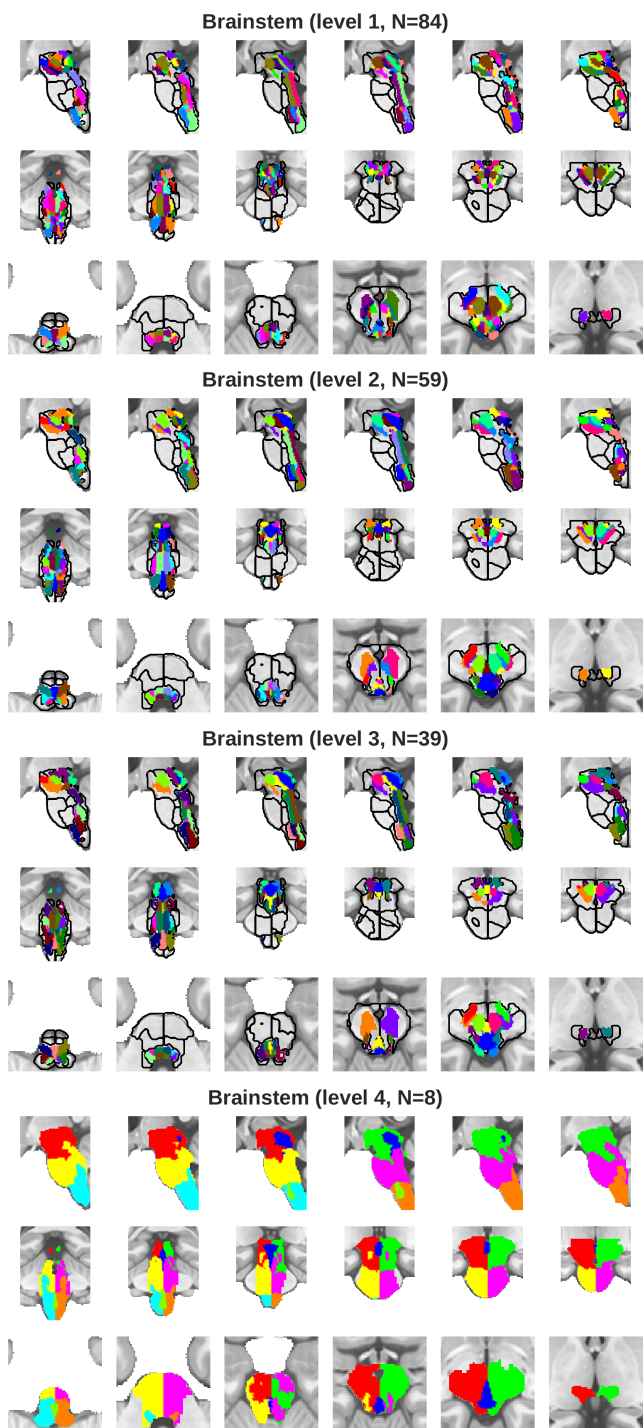


Figure 11: **CANLab2025 cerebellar parcels.** Level 1 (not shown) is identical to level 2.



**Figure 12: CANLab2025 differs from openCANLab2025 in the pons and medulla.** Openly licensed probabilistic regions are largely shared between the two atlases (multicolored). CANLab2025 includes a number of regions with distribution restrictions (black outlines) and can only be incorporated into the copy of openCANLab2025 we distribute after being downloaded from a licensed repository. As a substitute we provide a number of pontine and medullary regions in openCANLab2025 (orange) that are non-probabilistic, but have boundaries that roughly coincide with equivalent regions in CANLab2025. Finally, we provide a setup script which removes these regions, downloads the canlab2025 specific brainstem regions and inserts them appropriately to produce CANLab2025.



**Figure 13: CANLab2025 brainstem parcels.** The brainstem is a mixture of highly intermingled gray and white matter structures, and not all gray matter structures are yet available in MNI coordinate digital atlases. To provide comprehensive coverage of the brainstem we combined available parcellations (colored) with filler regions defined by resting state functional network boundaries (black outlines). At the coarsest level of granularity these two divisions are merged.